The Astrophysical Journal, 823:154 (9pp), 2016 June 1 doi:10.3847/0004-637X/823/2/154

THE ABSOLUTE RATE OF LGRB FORMATION

J. F. Graham and P. Schady
Max-Planck Institute for Extraterrestrial Physics, Giessenbachstrasse 1, D-85748 Garching, Germany
Received 2015 November 4; accepted 2016 February 15; published 2016 June 1

ABSTRACT

We estimate the long-duration gamma-ray burst (LGRB) progenitor rate using our recent work on the effects of environmental metallically on LGRB formation in concert with supernovae (SNe) statistics via an approach patterned loosely off the Drake equation. Beginning with the cosmic star formation history, we consider the expected number of broad-line Type Ic events (the SNe type associated with LGRBs) that are in low-metallicity host environments adjusted by the contribution of high-metallicity host environments at a much reduced rate. We then compare this estimate to the observed LGRB rate corrected for instrumental selection effects to provide a combined estimate of the efficiency fraction of these progenitors to produce LGRBs and the fraction of which are beamed in our direction. From this we estimate that an aligned LGRB occurs for approximately every 4000 ± 2000 low-metallically broad-lined SNe Ic. Therefore, if one assumes a semi-nominal beaming factor of 100, then only about one such supernova out of 40 produce an LGRB. Finally, we propose an off-axis LGRB search strategy of targeting only broad-line Type Ic events that occur in low-metallicity hosts for radio observation.

Key words: galaxies: star formation – gamma-ray burst: general – supernovae: general

1. INTRODUCTION

This is the second of two papers that look directly at the effect of environmental metallically on the long-duration gamma-ray burst (LGRB) rate. The first paper, Graham & Fruchter (2015), performs a relative comparison of the impact of host galaxy metallically on the rate of LGRBs per unit star formation available. Here, we look at the absolute LGRB rate using our knowledge of the effects of metallically on LGRB formation and the established connection between LGRBs and broad-line Type Ic (Ic-bl) supernovae (SNe; Modjaz et al. 2008).

Since the *BeppoSAX* detection of LGRB 980425 coincident in space and time with Type Ic supernova SN 1998bw (and the detection of LGRB 030329 with an optical afterglow on the exact position of its supernova) we have known that at least some LGRBs have an associated supernova event (Galama et al. 1999; Pian et al. 1999). However it was immediately obvious that not all SNe could result in LGRBs as there were nowhere near enough LGRBs for all the SNe even after correcting for the factor of LGRBs that were not beamed in our direction. As the population of LGRB SNe grew it became clear that they where not just associated with a particular type of SNe, Ic, but that the LGRB associated events had unusually broad spectral features (Modjaz et al. 2008). However without considering the impact of metallicity on the LGRB formation rate there remained too many of the specific broad-lined SNe Ic compared with too few LGRBs, even given the crude estimate of the latter. Even when considering the ∼30% of dark LGRBs (Perley et al. 2013) this discrepancy between Ic-bl SNe and LGRB numbers does not change in any significant way.

If we know the rate of LGRBs relative to other core-collapse events, then we can study the mechanisms required for LGRB formation. Three recent developments allow for a significant advance in this approach: Lien et al. (2014) has exhaustively analyzed the *Swift*-BATs performance to estimate the true GRB rate, Graham & Fruchter (2013) show that observations of LGRBs mostly occurring in low-metallicity environments is a strong intrinsic preference; and Graham & Fruchter (2015) quantized this as most LGRBs occurring in the least metal-rich ∼10% of the star formation with LGRB events at higher metallicallies occurring less than 25 times as often per unit star formation.

Now with a much improved understanding of the LGRB rate and of the impact of environmental metallicity on LGRB formation we will conduct a more detailed analysis. Here we will begin, in Section 2, with the cosmic star formation rate (CSFR) history, correlate this to the supernova rate, and step though the selections necessary for a supernova to also give rise to an LGRB. In Section 3, we compare this predicted rate with the observed LGRB rate corrected for instrumental selection effects. We assess the difference between our analytically derived LGRB rate and observationally based LGRB rate, and what it tells us about LGRB progenitors.

2. A DRAKE EQUATION FOR LGRBS

Our analysis will begin with, $R_{\rm SF}$, the CSFR. Star formation has the advantage of being studied both for the local universe and across the universe's history. Since LGRB progenitors have short lifetimes, LGRBs trace the on-going star formation, and their cosmic rate should thus match the CSFR after taking into account the conditions necessary to form an LGRB. Estimates of the current CSFR, $R_{\rm SF}(z=0)$, are in reasonable agreement $0.0158^{+0.003}_{-0.004}$ (Hanish et al. 2006), 0.0193 ± 0.0012 (Horiuchi et al. 2011 analysis of Bothwell et al. 2011 data), 0.01729 ± 0.0035 (average of Bothwell et al. 2011 Table 3 literature values) $M_{\odot}\,{\rm yr}^{-1}\,{\rm Mpc}^{-3}$. We thus adopt a mean value of 0.0175 ± 0.0025 for $R_{\rm SF}(z=0)$.

To extend the CSFR as a function of redshift we adopt the piecewise Hopkins & Beacom (2006) model. This model fits the CSFR with a series of three power-law estimates across different redshift ranges roughly corresponding to $0 < z < 1$, $1 < z < 4.5$, and $z > 4.5$ (see Table 1). We believe the initial and middle pieces of this estimate to be reasonably well constrained observationally with the final $z \gtrsim 4.5$ term being highly uncertain (even Hopkins & Beacom 2006 increases there uncertainty in this region to >50%). Yüksel et al. (2008) have attempted to use LGRBs to probe the CSFR at $z \gtrsim 4$ and suggest a much reduced rate of decline and thus higher CSFR

Table 1
CSFR Parameters

Variable	Value
$R_{\rm SF}(z=0)$	0.0178
a	3.28
b	−0.26
c	−8.0
z_1	1.04
z_2	4.48
η	−10

Note. Hopkins & Beacom (2006) values for Equation (1). With the exception of $R_{\rm SF}(z=0)$ and η, these are a subset of the Salpeter (1955) IMF values in Hopkins & Beacom (2006) Table 2 (of these only the independent parameters needed for Equation (1) are shown).

than estimated in Hopkins & Beacom (2006). The Hopkins & Beacom (2006; and other conventional) CSFR estimates are based on fits to deep, multi-band galaxy observations, and the difference between CSFR at $z > 4$ derived from LGRBs and galaxy observations could be the result of a significant fraction of star formation at $z > 4$ occurring in low-luminosity, low-mass galaxies that are undetected in traditional galaxy surveys. However, Robertson & Ellis (2012) claim that such an LGRB determined high-redshift SFR would overpredict the observed stellar mass density and thus the LGRB production rate (at least at $z > 4$) may be effected by factors other than SFR and environmental metallicity. To avoid these issues altogether we will look only at the CSFR in the initial and middle piecewise power-law terms. We adopt the functional CSFR form of Yüksel et al. (2008) along with the $\eta = -10$ smoothing term, as shown in Equation (1), but to prevent circular reasoning (i.e., using an LGRB based CSFR to estimate the LGRB rate) we retain the Hopkins & Beacom (2006) values as shown in Table 1.

$$R_{\rm SF}(z) = R_{\rm SF}(z=0)\left[(1+z)^{a\eta} + \left(\frac{1+z}{(1+z_1)^{1-a/b}}\right)^{b\eta} + \left(\frac{1+z}{(1+z_1)^{(b-a)/c}(1+z_2)^{1-b/c}}\right)^{c\eta}\right]^{1/\eta}. \quad (1)$$

Then we will consider the steps necessary to convert star formation to LGRBs. As it is often more convenient to think in numbers that are greater than 1 we will throughout this work refer to the reciprocals of these fractions as factors, f^{-1}. For instance if a nominal 1 out of 100 LGRBs are oriented in our direction this would correspond to a beaming fraction of $f_b = 0.01$ or a beaming factor of $f_b^{-1} = 100$. We will also adopt a uniform ΛCDM cosmology of $\Omega_M = 0.27$, $\Omega_\Lambda = 0.73$, and $H_\circ = 71$. As Hopkins & Beacom (2006) assume a modified Salpeter (1955) A IMF (Baldry & Glazebrook 2003) we will also adopt this IMF.

Given the connection between GRBs and SNe, the first step is to derive the fraction, $f_{\rm cc/SF}$, of core-collapse SNe created per $M_\odot$ of star formation. This is estimated (for the Salpeter 1955 IMF) as 0.0070 in Horiuchi et al. (2009) but without a reported error. This, applied to our $R_{\rm SF}(z=0)$ value, gives us a predicted core-collapse SNe rate, $R_{\rm cc}$, of $1.2 \pm 0.2 \times 10^5\,{\rm yr}^{-1}\,{\rm Gpc}^{-3}$. Along with its near corollary the SNe II rate, the cc SNe has been well studied and a number of estimates exist in the literature. Horiuchi et al. (2011) identified a systematic factor of 2 mismatch between a higher SN rate as estimated from the SFR and the lower directly observed SN rate. Using a conversion factor of 1 supernova per $114\,M_\odot$ of star formation (as observed in smaller host galaxies) Horiuchi et al. (2011) estimates a local cc SNe rate of $1.4 \times 10^5\,{\rm yr}^{-1}\,{\rm Gpc}^{-3}$ based on the SFR of the local universe. This agrees well with the SNe II rate of 1.1×10^5 from Lien & Fields (2009) using similar methodology, but not with the observed cc SNe rate of $7.05^{+1.65}_{-1.49} \times 10^4\,{\rm yr}^{-1}\,{\rm Gpc}^{-3}$ of Li et al. (2011) in a nearby sample of relatively large galaxies. Horiuchi et al. (2011) believes this discrepancy can be explained due the SNe being optically dim, either intrinsically or due to dust. This is consistent with observations of ∼30% of LGRBs being dark[1] (Perley et al. 2009; Greiner et al. 2011), since we would expect a lower rate of extinction in the smaller metal-poor LGRB host population. Thus we believe this factor of ∼2 difference in SNe rates is indeed due to extinction and thus accept the higher SFR inferred cc SNe rate as correct. We assume that the error between our predicted $R_{\rm cc}$ value and the Horiuchi et al. (2011) estimate is due the error in the $f_{\rm cc/SF}$ and thus adopt a value with error of 0.007 ± 0.001 for $f_{\rm cc/SF}$.

Next we consider the fraction, $f_{\rm Ibc/cc}$, of cc SNe that are Type Ib or Ic which are collectively referred to as Type Ibc. For these estimates we require a large homogenous sample of well typed SNe devoid of systematic effects or other biases. Therefore we appropriate the SNe populations of Kelly & Kirshner (2012) Figure 1 and compare the number of SNe between the different types therein using this as a representative population. We also assume Poisson statistics and thus assume the square root of the number of events as the error. This gives $f_{\rm Ibc/cc}$ values of 0.203 ± 0.031 and 0.228 ± 0.027 for galaxy-impartial and galaxy-targeted survey populations, respectively. As these agree within errors we adopt the combined value of 0.218 ± 0.021 for $f_{\rm Ibc/cc}$ and assume that any difference between the survey populations will be inherently most significant between SNe I and II given their difference in brightness. Notably Li et al. (2011) gives a direct estimate of the SN Ibc rate of $2.58^{+0.728}_{-0.716} \times 10^4\,{\rm yr}^{-1}\,{\rm Gpc}^{-3}$, which is actually in rather good agreement with the $\sim 3 \times 10^4\,{\rm yr}^{-1}\,{\rm Gpc}^{-3}$ rate we estimate using our $R_{\rm SF}$, $f_{\rm cc/SF}$, and $f_{\rm Ibc/cc}$ values. This is in contrast to the factor of 2 disagreement between the cc SNe rate derived from observations and from the CSFR. SNe I are typically about a magnitude brighter than SNe II, which reduces the selection effects introduced by e.g., dust, and the observed and modeled SNe I rate are thus in closer agreement.

Next we consider the fraction, $f_{\rm Ic/Ibc}$, of Type Ibc events that are Type Ic. Using the combined galaxy-impartial and galaxy-targeted Kelly & Kirshner (2012) populations gives a value of 0.69 ± 0.09 for $f_{\rm Ic/Ibc}$. We consider the $f_{\rm Ibc/cc}$ and $f_{\rm Ic/Ibc}$ fractions separately due to the additional difficulty in separating Ib and Ic types which involves determining the presence or absence of the 5876 Å He I line. This process is usually omitted from searches interested in identifying Type Ia events and also usually requires later time spectroscopy than is needed to identify the presence or absence of the hydrogen and silicon features used to distinguish between Type I or II and Ia or Ibc SNe, respectively. Additionally, by considering the combined fraction of Type Ibc events, it is possible to use SNe II rate

[1] Dark bursts lack an observed optical counterpart presumably because of extinction.

Table 2
Table of Values for Equation (2)

Variable	Description	Value	Source
$f_{cc/SF}$	Number of cc SNe per $M_\odot$ of SF	0.007 ± 0.001	Horiuchi et al. (2009)
R_{cc}	Local rate of core collapse SNe[g]	$1.4 \pm 0.1 \times 10^{5}$[i]	Horiuchi et al. (2011)
$f_{Ibc/cc}$	Fraction of core collapse SNe that are Ibc's	0.22[d] ± 0.02[a]	Kelly & Kirshner (2012)
$f_{Ic/Ibc}$	Fraction of Ibc's that are Ic's	0.69[d] ± 0.09[a]	Kelly & Kirshner (2012)
$f_{Ic\text{-}bl/Ic}$	Fraction of Ic's that are broad-line	0.21[d] ± 0.05[a]	Kelly & Kirshner (2012)
Z^+	Low-metallicity star formation fraction	$0.1^{+0.1}_{-0.05}$[c]	Graham & Fruchter (2013)
R_{RF}	Metallicity relative rate factor	$\sim$30 or $>$25	Graham & Fruchter (2015)
f_{eff}	Efficiency fraction	Unknown	...
f[b]	Beaming fraction	0.0019 ± 0.0003 0.013 ± 0.004	Frail et al. (2001) Guetta et al. (2005)
R_{aLGRB}	Local rate of aligned LGRBs[g]	$0.42^{+0.9}_{-0.4}$	Lien et al. (2015)
N_{aLGRB}	Total number of aligned LGRBs[b]	4568^{+825}_{-1429}[e]	Lien et al. (2015)
$Z^+ = 1 - Z^-$	High-metallicity star formation fraction	$0.9^{+0.1}_{-0.05}$[c]	Calculated from above
$f_Z = Z^- + Z^+/R_{RF}$	Adjusted environmental fraction	$0.13^{+0.1}_{-0.05}$	Calculated from above
$f_{Ic\text{-}bl/Ibc} = f_{Ic/Ibc} \times f_{Ic\text{-}bl/Ic}$	Fraction of Ibc's that are broad-line Ic's	$\approx$0.07 0.14[e] $\pm$ 0.04	Guetta et al. (2005) Calculated from above
$f_{Ic\text{-}bl/cc}$	Fraction of core collapse SNe that are Ic-bl	0.032 ± 0.007	Calculated from above
$f_{ceb}^{-1} = f_{eff}^{-1} \times f_b^{-1}$	Combined efficiency and beaming fraction	4000 ± 2000	this paper—Section 3.4

Notes.
[a] Assumed to be Poisson therefore standard deviation is estimated as the square root of the counts.
[b] Across all redshifts.
[c] Value for redshift zero only.
[d] Calculated from totals across both plots in Kelly & Kirshner's (2012) Figure 1. These plots are assumed to be a representative population.
[e] Value for entire universe.
[f] The lack of undiscriminated Type Ibc's does pose the question if these events are under represented.
[g] Value for local universe per GPc per year.

Table 3
Metallicity Evolution Cases Evaluated

Metallicity Evolution Case	Plot Color	Normalized Least Squares Residual	χ^2/dof
$Z^+_{n+1} = Z^+_n + a \times CSFR_n$	purple	1.21	3.87/7
$Z^+_{n+1} = Z^+_n + a \times CSFR_n \times (1 + z_n)$	blue	1.02	3.33/7
$Z^+_{n+1} = Z^+_n + a \times CSFR_n \times (1 + z_n)^3$	cyan	0.88	2.74/7
$Z^+_{n+1} = Z^+_n + a \times CSFR_n \times Z^-_n$	yellow	0.94	3.11/7
$Z^+_{n+1} = Z^+_n + a \times CSFR_n \times (1 + z_n) \times Z^-_n$	orange	0.86	2.76/7
$Z^+_{n+1} = Z^+_n + a \times CSFR_n \times (1 + z_n)^3 \times Z^-_n$	red	1.34	3.33/7
$Z^+ = 0$ (i.e., no metallicity dependance)	black solid	4.48	9.73/7
Original Wanderman & Piran (2010) fit	black dashed	1	2.40/7

Note. Least squares and chi squared logarithmic errors of the various metallicity evolution cases (colored lines), the cosmic star formation rate history (black line), and the two piece pow-law fit of Wanderman & Piran (2010; dashed black line) with respect to the Wanderman & Piran (2010) data (gray points with error bars) as shown in Figure 3. This fitting and associated error computation is limited to the $0 < z < 4$ range so the slope of the poorly known final third high-redshift term in the Hopkins & Beacom (2006) CSFR history does not effect results.

estimates to determine the core-collapse SNe rate via $R_{II} = (1 - f_{Ibc/cc})\, R_{cc}$.

Next we consider the fraction, $f_{Ic\text{-}bl/Ic}$, of Type Ic events that have relativistic ejecta causing a noticeable Doppler broadening of their spectral features. Such broad-line features seem to be only associated with SNe Ic and are thought to be associated (like LGRBs) with central engine activity (Iwamoto et al. 1998). However, Graham & Fruchter (2013) showed that broad-line SNe Ic not only occur primarily at high metallically (Modjaz et al. 2008) but follow the metallically distribution of star formation in the general galaxy population, unlike LGRBs which occur much more frequently in low-metallically environments (Fruchter et al. 2006; Stanek et al. 2007; Wolf & Podsiadlowski 2007; Modjaz et al. 2008; Levesque et al. 2010a, 2010b; Graham & Fruchter 2013; Perley et al. 2015). Again we turn to the sample of Kelly & Kirshner (2012) which gives a value of 0.21 ± 0.05 for $f_{Ic\text{-}bl/Ic}$. As we are using the Kelly & Kirshner (2012) combined SNe survey population for all of our SNe fractional estimates, we can also directly estimate the fraction of core-collapse SNe that are broad-line SNe Ic events, $f_{Ic\text{-}bl/cc}$, without considering the intermediate steps, giving a value of 0.032 ± 0.007. However these intermediate steps likely contain information on the physical processes that give rise to LGRBs, so we will retain

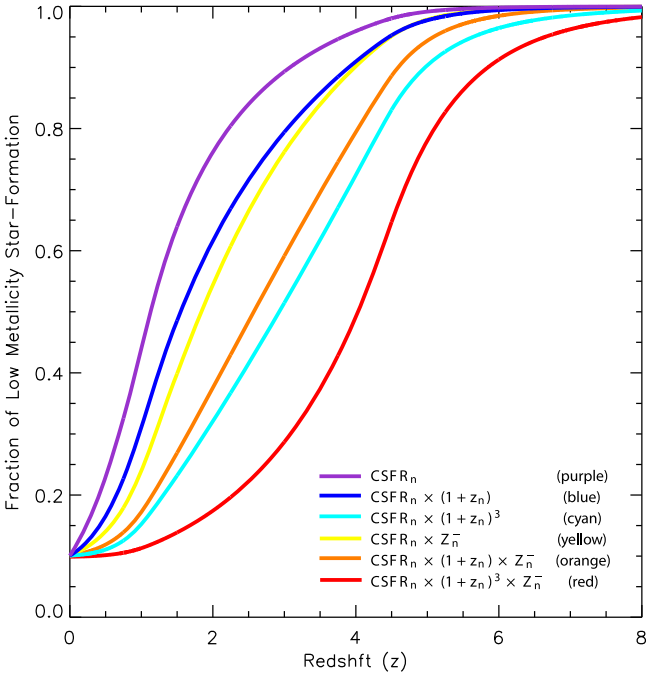

Figure 1. Fraction of low metallicity ($\log(\mathrm{O/H}) + 12 < 8.4$ in the KK04 scale) as a function of redshift, $Z^-(z)$, for the different cases of metallicity evolution determined by iterating the relationships given in Equation (4) such that $Z^+(z = 0) = 0.9$ and $Z^+(z = 20) = 0$. We believe these 6 cases provide a reasonable distribution of possibilities for the evolution of metallicity with redshift.

them in our analysis. Also the individual steps can be more easily compared to current and future SNe surveys than just using the $f_{\mathrm{Ic\text{-}bl/cc}}$ value, and consequently improved upon.

Next we must represent the preference of LGRBs for low-metallicity environments (Fruchter et al. 2006; Stanek et al. 2007; Wolf & Podsiadlowski 2007; Modjaz et al. 2008; Levesque et al. 2010a, 2010b; Graham & Fruchter 2013; Perley et al. 2015). However there are some LGRBs that do at least appear to occur in high-metallically environments (Graham et al. 2009, 2015; Levesque et al. 2010c; Graham & Fruchter 2013). In Graham & Fruchter (2015) we find there to be a sharp cut-off at $\log(\mathrm{O/H}) + 12 \sim 8.3$ above which the GRB formation rate drops by about a factor of ~30. This result agrees roughly with the burst redshift distribution constraints (for the case of a constant burst luminosity function) of Salvaterra & Chincarini (2007), Salvaterra et al. (2012), and Butler et al. (2010). Even if the LGRB rate in high-metallicity environments is in fact zero, and LGRBs with high-metallicity hosts occur in low-metallically pockets, we would still need to account for the LGRBs that occur in what we measure to be high-metallically host galaxies. Fortunately this distinction is not only immaterial to this analysis but suggests how we can simply accommodate these exceptions into our fractional methodology. We treat the high-metallically LGRBs as if they were also due to additional low-metallically star formation and adjust the fraction accordingly. Here we represent the fraction of cosmic star formation at low metallically ($\log[\mathrm{O/H}] + 12 < 8.4$ in the Kobulnicky & Kewley 2004, henceforth KK04, scale) as Z^-, and its corollary the fraction at high-metallically star formation as Z^+ (such that $Z^- + Z^+ = 1$). Thus we calculate the environmental fraction, f_Z, of adjusted low-metallically star formation by adding to the observed fraction of low-metallically star formation, Z^-, the fraction of high-metallically star formation divided by the relative rate factor, R_{RF}. The relative rate factor is the rate (per unit star formation) at which we produce LGRBs in low-metallically environments divided by the rate at which we produce LGRBs in high-metallically environments. This yields $f_Z = Z^- + Z^+/R_{\mathrm{RF}}$. We calculated the R_{RF} to be at least 20 and most likely greater than 30 in Graham & Fruchter (2015). Assuming $R_{\mathrm{RF}} = 30$ and the value of $Z^- = 0.1^{+0.1}_{-0.05}$ that we estimated from an observational comparison of the distributions LGRB and star formation with metallically in Graham & Fruchter (2013), gives an adjusted value of $f_Z = 0.13^{+0.1}_{-0.05}$ for the local universe. The f_Z can be thought of as the fraction of low-metallically star formation required if all LGRBs are being formed in low-metallically environments.

Given that not all broad-line SNe Ic, even those in low-metallically environments, necessarily generate an LGRB, we add an efficiency fraction, f_{eff}, to represent the fraction that do, and which effectively contains our lack of understanding on what precise progenitor conditions result in an LGRB. Given that we do not fully understand the exact progenitor properties that lead to a broad-line SNe Ic being accompanied by an LGRB, estimating this efficiency fraction is the principal motivation of this paper.

In order to consider only LGRBs aligned in our direction we must further consider the beaming fraction, f_b given by the burst's beaming angle. There are two wildly different values for f_b^{-1} of 520 ± 85 and 75 ± 25 from Frail et al. (2001) and Guetta et al. (2005), respectively. The different values are calculated via different methodologies. The primary difference being that the Guetta et al. (2005) method assumes the existence of a large number of low-luminosity bursts which cannot be observed except at the closest redshifts (see Piran 2005 for a more detailed yet still brief comparison of the two methodologies). We also note the consistency between the beaming angle of the Frail et al. (2001) population (see their Figure 1) with that of the *Swift* population (see Ryan et al. 2015 Figure 4). However, the Frail et al. (2001) methodology makes certain simplifications in their assumed jet structure and assumes any optical break to be a jet break, which is now known to be a poor approximation. Racusin et al. (2009) analyzed the X-ray afterglows of two years of *Swift* GRBs (~250 objects) using the relation between the spectral and light curve slopes to determine which breaks in the X-ray light curves were likely jet breaks, and in these cases derived the jet opening angle. One issue is that to determine the jet angle, one of the parameters that is required is the GRB isotropic-equivalent energy release, E_{iso}. This requires the burst redshift to be known and thus is not available for most LGRBs. Even in those cases where E_{iso} is known, the range in opening angles is fairly large, and the sample sizes appear insufficient to confidently determine a distribution, and thus the mean angle. For example Gao & Dai (2010) looked at the jet opening angles for a sample of 28 long GRBs, and they found the mean and standard deviation to be $3^\circ.42 \pm 9^\circ.07$!

$$R_{\mathrm{aLGRB}} = R_{\mathrm{SF}} \times f_{\mathrm{cc/SF}} \times f_{\mathrm{Ibc/cc}} \times f_{\mathrm{Ic/Ibc}} \times f_{\mathrm{Ic\text{-}bl/Ic}} \times \left(Z^- + \frac{Z^+}{R_{\mathrm{RF}}}\right) \times f_{\mathrm{eff}} \times f_b\,. \quad (2)$$

This process yields Equation (2). Since there is considerable uncertainty in the beaming fraction and the efficiency fraction is unknown we will combine the opening angle and efficiency into a single unknown parameter, the combined efficiency and

beaming fraction, $f_{\rm ceb}$, so that we can provide estimates that will allow the reader to easily estimate the efficiency fraction with their choice of beaming fraction (i.e., $f_{\rm ceb} = f_{\rm eff} \times f_b$). This along with a simplification of the SNe fractions yields Equation (3):

$$R_{\rm aLGRB} = R_{\rm SF} \times f_{\rm cc/SF} \times f_{\rm Ic\text{-}bl/cc} \times \left(Z^- + \frac{Z^+}{R_{\rm RF}}\right) \times f_{\rm ceb}\,. \quad (3)$$

Values for the variables in Equations (2) and (3) are provided in Table 2.

3. THE COSMIC LGRB AND SFR RATES

Altogether these steps produce Equations (2) and (3), which gives an estimate of the rate of aligned LGRBs and has a notable similarity to the Drake equation for estimating the number of inhabited extrasolar planets in our galaxy. Unlike the Drake equation however this equation has the considerable advantage of the aligned LGRB rate, $R_{\rm aLGRB}$, now being reasonably well known thanks to the seminal work of Lien et al. (2014; revised in Lien et al. 2015 and expanded in Graff et al. 2015). Their detailed analysis and simulation of the *Swift* BAT detector gives a rate of $0.42\,{\rm yr}^{-1}\,{\rm Gpc}^{-3}$ for aligned LGRB events in the local universe (Lien et al. 2015). Unfortunately, as we will address in Section 3.2, the parametric forms of the local LGRB and CSFR are sufficiently different to preclude our believing this "local" rate is truly representative at $z < 1$. Nevertheless, Lien et al. (2014), and in a comparable but updated analysis, Graff et al. (2015), provide reasonable observational estimates on the LGRB rate as a function of redshift (at least in the $1 < z < 4$ range).

3.1. The Evolution of Metallicity

Understanding the evolution of the low-metallicity star formation fraction (Z^-) with redshift is complicated and a task we hope to address in upcoming work. While there are some existing observational (Yuan et al. 2013; Zahid et al. 2013) and theoretical (Yates et al. 2012) efforts to understand metallicity evolution with redshift, none of them enable us to estimate the Z^- term as a function of redshift. What we need is a census of the distribution of star formation below a set metallicity cutoff throughout the universe as a function of redshift. While we hope to address this with simulations and perhaps observations in a future work, for now however we can place some constraints with our existing knowledge and will attempt some estimates based on first principles. Furthermore by trying and then evaluating a diverse range of possibilities we may be able to shed some insight on the evolution of metallicity itself.

As determined in Graham & Fruchter (2013), we know that the $Z^+_{\rm now} \approx 0.9$ in the local universe and we can assume that $Z^+_\circ = 0$ primordially. Furthermore as metal production is the result of star formation we can assume that the rise in Z^+ should correspond to the integral of the CSFR. The remaining question is what other factors will effect the relationship between metallicity enhancement and star formation. Ideally we would consider not only the creation of metals (i.e., star formation) but also account for the removal and dilution of metals by outflows and inflows. Given the uncertainties in the effect of outflows and inflows, and that these are most likely second order effects, we only consider the effect on metallicity evolution from Z^+ and z. Thus we consider only the effects of the scale factor and of the current metallicity on the efficiency of star formation in increasing the fraction of high-metallicity star formation (i.e., $\log({\rm O/H}) + 12 > 8.3$ in KK04 scale). For the scale factor we consider that the efficiency of star formation in increasing the metal content of the universe might increase by a factor of $(1+z)$ or $(1+z)^3$ (and also that scale factor might play no role in metal enrichment efficiency). The factor of $(1+z)$ takes into account the compression of the universe, and the factor of $(1+z)^3$ corresponds to the increase in the specific SFR, both of which we can reasonably imagine would effect the evolution of Z^-. It is important to factor in that once gas enrichment reaches a certain metallicity, the star formation at low metallicity will no longer increase, at least if we assume that mixing is inefficient. Thus the effect of SFR on the increase of Z^+ would effectively be reduced by a factor of Z^+. That is, when at some point a third of the universe has been enriched to high metallicity we assume that star formation will only be two-thirds as effective at metal enrichment as when $Z^+ = 0$. Of course if the universe is well mixed than super enriched gas would still contribute as it became diluted by metal-poor gas. This gives us six relationships to test: CSFR, CSFR $\times (1+z)$, CSFR $\times (1+z)^3$, CSFR $\times Z^-(z)$, CSFR $\times (1+z) \times Z^-(z)$, CSFR $\times (1+z)^3 \times Z^-(z)$,

$$\begin{aligned}
Z^+_{n+1} &= Z^+_n + a \times {\rm CSFR}_n && \text{(purple)}\\
Z^+_{n+1} &= Z^+_n + a \times {\rm CSFR}_n \times (1+z_n) && \text{(blue)}\\
Z^+_{n+1} &= Z^+_n + a \times {\rm CSFR}_n \times (1+z_n)^3 && \text{(cyan)}\\
Z^+_{n+1} &= Z^+_n + a \times {\rm CSFR}_n \times Z^-_n && \text{(yellow)}\\
Z^+_{n+1} &= Z^+_n + a \times {\rm CSFR}_n \times (1+z_n) \times Z^-_n && \text{(orange)}\\
Z^+_{n+1} &= Z^+_n + a \times {\rm CSFR}_n \times (1+z_n)^3 \times Z^-_n && \text{(red).} \quad (4)
\end{aligned}$$

We thus iterate these relationships in the form of Equation (4) in million year increments from $z = 20$ to now (assuming $Z^+_{z=20} = 0$) with the constant a selected (for each relationship) such that $Z^+_{\rm now} = 0.9 \pm 0.001$, with the results shown in Figure 1 (this error represents only the tolerance used in determining the a values). As each of these relationships form a distinct metallicity evolution test case we find it useful to assign a name to each case—for simplicity and lack of a short physically descriptive names we assign names to the metallicity evolution cases corresponding to the colors we use to plot them in the figures.

3.2. Difficulties in Estimating the Local LGRB Rate

Broken power-law estimates of the CSFR(z) give an initial evolution of $(1+z)^x$ with x being about 3.4 (Hopkins & Beacom 2006) whereas estimates of the LGRB rate (typically fit from now out to z of 3 or 4) go with x being about 2.1 (Wanderman & Piran 2010; Lien et al. 2014). As a result of the small number of LGRBs at $z < 1$, any functional form fitted to the LGRB is very poorly constrained in this range. A simple power law is commonly assumed, where the LGRB rate at $1 < z < 3$ weighs more heavily. While one might expect metallicity evolution to be able to explain the CSFR versus LGRB rate slope difference, metallicity evolution actually acts in the opposite direction (assuming of course that the metal content of the universe can only increase with time). Assuming that the LGRB rate must follow the CSFR (with some enhancement at low metallicities), this suggests that the fitted $z = 0$ LGRB rate is over estimated by at least a factor of 2

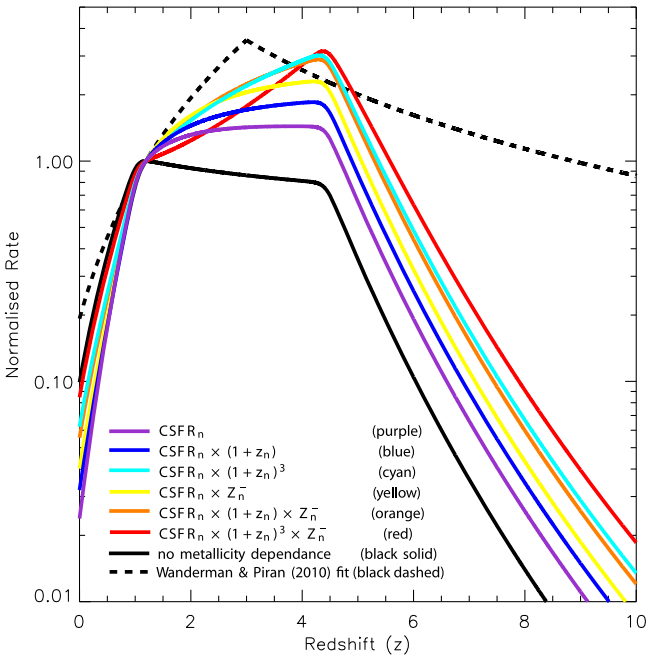

Figure 2. CSFR at low metallicity (colored lines) as a function of redshift compared with the total CSFR (black solid line) and the LGRB rate estimates of Wanderman & Piran (2010; dashed solid line) with all values normalized at the redshift of the CSFR peak ($z \approx 1.2$). The CSFR at low metallicity is determined as the product of the CSFR and our low-metallicity fraction estimates, $Z^-(z)$, from Equation (4) as shown in Figure 1.

when the LGRB rate is estimated as a continuous power law out to $z \sim 3$. This discrepancy between the observed LGRB rate extrapolated down to $z = 0$ and the lower LGRB expected from the CSFR is not particularly observable because of the large statistical uncertainty on the observed local rate due to LGRBs being relatively rare events. In general, the nearby (non sub-luminous) LGRB rate is low, for example there are only 5 LGRBs (with $E_{\rm iso} > 10^{50}$ erg) at $z < 0.3$. Also, as shown in Figure 2, while the CSFR is only 50% of the normalized LGRB rate estimates of Wanderman & Piran (2010), by redshift $z = 0.3$ this difference is only 70%, and at $z = 0.5$ it is almost negligible. There is therefore little constraint to the functional form fitted to the LGRB rate at $z \lesssim 1$ and thus the functional form adopted is usually a single power-law fit in the $0 < z \lesssim 3$ range. By contrast the CSFR(z) seems to undergo a radical ~3.5 difference in power-law slope at $z \approx 1$. Since there are far more LGRBs in the $1 < z < 3$ range than the $0 < z < 1$ range, the tendency is to compare and normalize the LGRB rate and the CSFR in this range.

In Figure 2, we show the $(1 + z)^{2.1}$ LGRB rate of Wanderman & Piran (2010) along with the CSFR(z) of Hopkins & Beacom (2006). In addition, we show the CSFR (z) convolved with our 6 low-metallicity evolution functions described in Section 3.1 (see Figure 1). All plotted curves are normalized to unity at the peak redshift of the CSFR ($z \approx 1.2$). All the CSFR based LGRB estimates are thus at least a factor of two lower than the $0 < z < 3$ power-law fit of Hopkins & Beacom (2006). Given the limited number of LGRBs in the $0 < z < 1$ range we believe that the LGRB rate does indeed drop as the CSFR based estimates predict, but as the LGRB rate is relatively unconstrained in this region, usually the simplest model is fitted. Furthermore estimates of the $z = 0$ LGRB rate (c.f. Wanderman & Piran 2010; Lien et al. 2014; Graff et al. 2015; etc.) that do not take this into account (as Butler et al. 2010 did) will be systemically over estimated.

To avoid falling victim to this trap ourselves we will not attempt to compare the LGRB and CSFR rates at $z = 0$ despite the local universe being the only region where we have observational information on the distribution of star formation with metallicity. Instead we will use our metallicity evolution models from Section 3.1 to preform this analysis at $z > 1$ where both the CSFR(z) and the LGRB rate is well known.

3.3. LGRB Rate and Low metallicity CSFR Redshift Evolution

Now that we have estimates for the cosmic low-metallicity SFR, the next step is to compare them with the LGRB rate as a function of redshift. The latter has been estimated in Wanderman & Piran (2010) and Butler et al. (2010). Here we will primarily use the Wanderman & Piran (2010) data for comparison as its methodology of binning LGRBs by redshift is more easily reproducible and comparable to our methodology. We restrict our fitting to the redshifts below 4 to avoid being significantly affected by the slope of the high-redshift term in the Hopkins & Beacom (2006) piecewise power-law CSFR estimate, which becomes highly uncertain at $z > 4$. The approach is almost identical to that shown in Figure 2 except that instead of normalizing our values at a common redshift, here we will normalize each metallicity evolution case such that it provides the lowest least squares fit with the Wanderman & Piran (2010) data.

We find that 3 of our metallicity evolution cases provide a better least squares fit to the Wanderman & Piran (2010) data than the two step broken power-law fit given in Wanderman & Piran (2010; with an additional forth case with comparable error; see Table 3). This strongly suggests that metallicity evolution can explain the distribution of LGRBs as a product of the CSFR history, at least out to $z \sim 4$. A similar conclusion was suggested in Butler et al. (2010). While we can exclude the CSFR history without a metallicity dependance (black solid line in Figure 3), all of our metallicity evolution models fit the data rather well with the cyan and orange models performing the best. Having established a general consistency in shape between the data and our model across redshift, we will now apply the methodology of Section 2 to numerically compare the LGRB rate and CSFR history. Essentially the remaining exercise is one of scaling.

3.4. Comparing the Number of LGRB and Their Progenitors

While Wanderman & Piran (2010) and Butler et al. (2010) have looked at the distribution of LGRBs with redshift, an alternate approach pioneered in Lien et al. (2014) is to fully simulate the *Swift* Burst Alert Telescope (BAT) performance on a set of synthetic LGRB events varying their number, redshift distribution, and overall parameters so as to reproduce the observed *Swift* population. The large number of *Swift* events with measured redshifts allows this technique to be employed on the *Swift* LGRB redshift distribution, whereas it would not have been feasible on the much smaller collection of GRBs with known redshifts from all other missions combined. However the primary advantage of the Lien et al. (2014) methodology is that it allows not just an assessment of the redshift distribution of LGRBs but also their absolute number. However, while Lien et al. (2014) assumes a rather

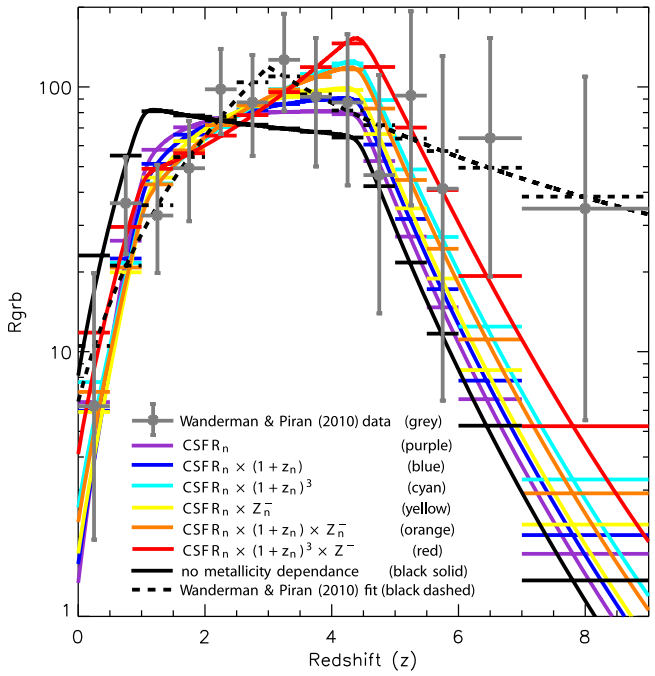

Figure 3. Here we repeat the plotting in Figure 2 except now normalize all lines to the logarithmic best fit in the $0 < z < 4$ range of the Wanderman & Piran (2010) rate estimates shown in gray. As this requires binning all the lines into histograms for fitting, additional horizontal bars of matching color indicate the level in each bin. As the binning process accounts for the change in comoving volume of the universe within individual bins, the matching lines and bars do not strictly intersect in the center of the bins.

conventional cosmic LGRB rate described by a fixed piecewise power-law with the pieces meeting at $z = 3.6$, and an initial power-law slope almost identical to that of Wanderman & Piran (2010), this methodology was expanded in Graff et al. (2015) to allow much more flexibility in fitting parameters.

Thus we compare the amount of low-metallicity star formation in the universe (as a function of redshift) with the Lien et al. (2014) and the Graff et al. (2015) estimates, using Equation (3) to estimate the combined efficiency and beaming factor, $f_{\rm ceb}^{-1}$, since all the other parameters are reasonably well known. We limit this comparison to redshifts above 1 because the LGRB rate is fairly unconstrained at $z < 1$ due to small number statistics (see Section 3.2). As before we also limit this comparison to redshifts below 4 as the slope of the CSFR at higher redshift is poorly known. This has the added advantage of mostly excluding the slope of the post peak decline in the LGRB rate, which has quite high uncertainties.

In Table 4 we solve for the $f_{\rm ceb}^{-1}$ value for each of our different metallicity evolution cases, using the LGRB predicted rates from the model of Lien et al. (2014) and the three machine learning models of Graff et al. (2015). As the shape of the low-metallicity star formation does not perfectly match the LGRB rate estimates, the resulting $f_{\rm ceb}^{-1}$ estimate varies slightly with redshift. We thus present the average and standard deviation of $f_{\rm ceb}^{-1}$ across the $1 < z < 4$ range. We note that two of the metallicity evolution cases (colored cyan and orange) give errors ∼12% whereas the other models give errors on the order of 30%–40%. Using both of these cases across all three Graff et al. (2015) methods (the bold values in Table 4) we estimate a $f_{\rm ceb}^{-1}$ value of 4048 ± 550. This is notably higher than the 3135 ± 668 estimated from the Lien et al. (2014) numbers for these same two metallicity evolution cases. (These errors are derived from the values given in Table 4 only.) Given this discrepancy as well as the 25% error in estimating the number of SNe Ic-bl per $M_\odot$ of star formation, and the accuracy limitations of the CSFR history itself, we adopt a value of 4000 ± 2000 as a reasonable estimate of our combined efficiency and beaming fraction.

4. FUTURE WORK

There is considerable room for improvement in almost every aspect of this analysis. Our goal here has been to outline the general methodology and do an initial quick employment of it using information conveniently available in the existing literature. By far the largest uncertainty is in the beaming factor estimations for LGRBs. We have attempted to largely sidestep this here by treating the efficiency of forming LGRBs and the degree to which they are beamed as a combined unknown to solve for and allowing the reader to easily use their own preferred beaming estimates. However an average beaming angle might not be particularly useful as the beaming angle distribution might also vary with the burst luminosity. Ghirlanda et al. (2013) suggests a factor of ∼2 smaller opening angle among the typically brightest bursts compared with the typical angle for bursts of average luminosity. Obviously a greater understanding of beaming would thus improve our understanding of LGRB production efficiency. Ultimately an expansion of the Lien et al. (2014)/Graff et al. (2015) simulations to all LGRB orientations with proper modeling of the off axis gamma emissions is desirable. Presumably such an expansion would require an increase of computing effort roughly equivalent to the beaming factor (approximately two orders of magnitude). However with reasonable thresholding prior to detector convolution (i.e., quickly discarding the majority of events obviously too weak for any chance of detection) it might be possible to limit the computational increase to less than an order of magnitude.

A more eminently practical expansion of the Lien et al. (2014)/Graff et al. (2015) simulations would be to switch from modeling parameters for arbitrary broken power-law LGRB rates to modeling functional forms more related to the CSFR and metallicity evolution of the universe. Our current approach of comparing the LGRB event rates estimated by these broken power-law functional forms to our estimated low-metallicity CSFR provides a reasonable approximation. However directly modeling an LGRB event rate from the low-metallicity CSFR will likely yield some improvement, as it will be physically motivated. Such an approach should allow for a better overall fit between the predicted and measured LGRB redshift distribution.

Additionally the existing observational studies of the LGRB redshift distribution from, Wanderman & Piran (2010), Butler et al. (2010) and the Fynbo et al. (2009; used in the Lien et al. 2014/Graff et al. 2015 simulations), date from 2010 or earlier. The number of *Swift* BAT LGRB detections has since more than doubled. There are now more then 400 LGRBs with known redshifts.[2] Assuming selection effects could be properly addressed, an analysis of this larger sample would considerably improve the precision on the redshift distribution of bursts which *Swift* detected and should thus allow a more accurate understanding of the true LGRB redshift distribution both in its shape and scaling.

[2] http://www.mpe.mpg.de/~jcg/grbgen.html

Table 4
f_{ceb} Estimates for Each Metallicity Evolution Case

Metallicity Evolution Case	Plot Color	Lien et al. (2015)	Graff et al. (2015)		
			RF	AB	NN
$Z^+_{n+1} = Z^+_n + a \times \mathrm{CSFR}_n$	purple	5786 ± 2316	7752 ± 2478	7776 ± 2449	7462 ± 2522
$Z^+_{n+1} = Z^+_n + a \times \mathrm{CSFR}_n \times (1+z_n)$	blue	4771 ± 1535	6432 ± 1571	6454 ± 1547	6184 ± 1601
$Z^+_{n+1} = Z^+_n + a \times \mathrm{CSFR}_n \times (1+z_n)^3$	cyan	2818 ± 532	**3836 ± 412**	**3851 ± 395**	**3687 ± 466**
$Z^+_{n+1} = Z^+_n + a \times \mathrm{CSFR}_n \times Z^-_n$	yellow	4266 ± 1070	5785 ± 1036	5807 ± 1014	5554 ± 1046
$Z^+_{n+1} = Z^+_n + a \times \mathrm{CSFR}_n \times (1+z_n) \times Z^-_n$	orange	3200 ± 610	**4357 ± 493**	**4375 ± 475**	**4186 ± 533**
$Z^+_{n+1} = Z^+_n + a \times \mathrm{CSFR}_n \times (1+z_n)^3 \times Z^-_n$	red	1770 ± 454	2397 ± 393	2407 ± 383	2312 ± 456

Note. f_{ceb} values for the different metallicity evolution cases and the different LGRB rate (function of redshift) estimates of Lien et al. (2014) and the three models (RF, AB, and NN) of Graff et al. (2015). As expected the cases with poor fitting in Figure 3/Table 3 is also have low accuracy here. The two best-fit cases are in bold.

Further observations of SNe Ic-bl events with and without associated LGRB events could prove particularly insightful especially if distinguishing properties can be identified in the SNe characteristics between these populations. However any such distinguishing property must be tested against a low-metallicity non-LGRB SNe Ic-bl population specifically. For example Cano (2013) claim that Ic-bl events with associated LGRBs are more energetic and eject more mass then those Ic-bl SNe without an associated LGRB. Yet it is unclear if this is due to the non-LGRB events being at typically higher metallicities or due to an intrinsic difference in central engine activity for LGRBs. The absence of any distinguishable difference in SNe properties with LGRB energy suggests a metallicity effect is more likely.

Finally a better understanding of the distribution of metallicity and its evolution with redshift is essential for furthering this work. Here we have resorted to testing six very simplistic first principle models for the evolution of the low-metallicity star formation fraction. Ideally this could be replaced with observational constraints. However a suitable population of uniformly selected high-redshift galaxies with measured metallicities is not available and it appears that the best hope for near-term improvement is with galaxy simulations along the lines of the L-GALAXIES semi-analytic model (Yates et al. 2012). Additionally being able to cross-calibrate and thus employ both emission and absorption metallicity diagnostics would greatly assist with tracking the expected eventual convergence of the LGRB and general galaxy population metallicity distribution once redshifts are high enough that the metallicity of the general galaxy population is as low as seen in typical LGRB hosts. Amusingly LGRBs are themselves likely to be the best events for backlighting absorption features in galaxies with strong emission features. Once the metallicity distributions of the LGRB and general galaxy populations have converged, it should be possible to use LGRBs as a probe of high-redshift star formation (c.f. Yüksel et al. 2008).

5. CONCLUSIONS

Here we have used the CSFR history (Hopkins & Beacom 2006), the core-collapse SNe production rate (Horiuchi et al. 2009), and the relative rates of different SNe types (Kelly & Kirshner 2012), along with estimates of metallicity evolution, distribution, and impact on LGRB production (Graham & Fruchter 2013, 2015) to derive a equation which estimates the LGRB rate in terms of a remaining unknown constant factor. This constant factor is a combination of the poorly known LGRB beaming factor and the unknown Ic-bl SN-to-LGRB efficiency factor in ideal low-metallicity environments. We then apply the LGRB rate estimates from simulations of the *Swift* BAT detector (Lien et al. 2014; Graff et al. 2015), which reproduce the observed *Swift* LGRB redshift rate and distribution (Fynbo et al. 2009; Wanderman & Piran 2010), to estimate that there are 4000 ± 2000 SNe Ic-bl in low-metallicity environments for every LGRB aligned in our direction. This number is a composite of the fraction of such SNe which produce LGRBs and the fraction that are beamed in our direction. We have ignored second order complexities such as LGRBs possibly not originating from SNe explosions, the canonical examples typically given as GRBs 060505 and 060614 (however GRB 060614 is generally considered a short burst, Dado et al. 2009; Bianco et al. 2012; Kaneko et al. 2015; etc. and 060505 is also disputed, Ofek et al. 2007), or LGRBs arising from non-broad-line SNe events, as has been claimed for GRB 130215A (SN 2013ez—Cano et al. 2014). Thus, assuming a semi-nominal beaming factor of 100, this would suggest that approximately 1 out of 40 low-metallically SNe Ic-bl events give rise to an LGRB.

These results are consistent with the absence of off axis LGRB detections in radio surveys of broad-line SNe Ic events. Given the 1 out of 40 rate estimated here, a sample size of about a hundred such (low metallicity) SNe would be required to be reasonably confident of detecting an off axis LGRB. The effect of metallicity on such searches is significant—a search performed without regard to metallicity will be about 5 times less effective in finding an LGRB. A search of the literature suggests that no such low-metallicity optimized off axis LGRB radio search has yet been conducted and that neither the singe low metallicity SNe Ic-bl in Graham & Fruchter (2013), SN 2007ce, or another event possibly at such low metallicity, SN 2006nx, have been subjected to such radio observations. Furthermore none of the SNe Ic-bl with sub-solar metallicities in Graham & Fruchter (2013) were found via a SNe search targeted at specific galaxies, and the median redshift of the non-targeted population $z = 0.0584$ exceeds the highest redshift of the targeted population. This suggests that such off axis LGRB searches may be biased toward SNe in high-metallicity galaxies and such an off axis search in high-metallicity environments will likely be about 30–60 times less effective in finding an LGRB (than a search in low-metallicity environments). This comparative degradation of search efficiency is independent on the beaming factor (however, the ideal 1 out of ∼40 factor is dependent on beaming angle).

A radio search focusing exclusively on SNe Ic-bl in environments with KK04 (Kobulnicky & Kewley 2004) metallicities of $\log(\mathrm{O/H}) + 12 < 8.4$ and containing ∼90 targets is thus recommended in the strongest possible terms in order to target off-axis LGRBs (with a ∼90% chance of detecting such an event). The current practicality of such an effort is questionable as finding 100 SNe Ic-bl will require typing ∼4000 SNe (based on the SNe type fractions given in Section 2 and Table 2 as well as the statistic of Li et al. 2011 that ∼25% of local SNe are Type Ia), all of which will need to be found in environments with only the lowest metallicity 10% of star formation and close enough to allow the required radio observations. We estimate approximately 150 SNe Ic-bl per year for the entire universe within $z < 0.05$, of which ∼15 will be in such low-metallicity environments. If recent advances in SNe search capabilities (i.e., Pan-STARRS, PTF, and the upcoming LSST) prove capable of finding about half of these events and are matched by a robust photometric SNe typing capability (to bring the needed spectroscopic observations down to a reasonable number) then it should be possible to find an off-axis LGRB within a decade of diligent searching and to place an $\mathrm{S/N} \sim 3$ estimate on the off-axis LGRB rate in a few decades.

We thank Andrew Fruchter, Jochen Greiner, Robert Yates, Hendrik van Eerten, David Alexander Kann, and in particular Amy Lien for useful discussions.

J.G. and P.S. acknowledge support through the Sofja Kovalevskaja Award to P.S. from the Alexander von Humboldt Foundation of Germany.

We also thank the anonymous referee for their kind and useful comments.

REFERENCES

Baldry, I. K., & Glazebrook, K. 2003, ApJ, 593, 258
Bianco, C. L., Amati, L., Bernardini, M. G., et al. 2012, MSAIS, 21, 139
Bothwell, M. S., Kenicutt, R. C., Johnson, B. D., et al. 2011, MNRAS, 415, 1815
Butler, N. R., Bloom, J. S., & Poznanski, D. 2010, ApJ, 711, 495
Cano, Z. 2013, MNRAS, 434, 1098
Cano, Z., de Ugarte Postigo, A., Pozanenko, A., et al. 2014, A&A, 568, A19
Dado, S., Dar, A., & De Rújula, A. 2009, ApJ, 693, 311
Frail, D. A., Kulkarni, S. R., Sari, R., et al. 2001, ApJL, 562, L55
Fruchter, A. S., Levan, A. J., Strolger, L., et al. 2006, Natur, 441, 463
Fynbo, J. P. U., Jakobsson, P., Prochaska, J. X., et al. 2009, ApJS, 185, 526
Galama, T. J., Vreeswijk, P. M., van Paradijs, J., et al. 1999, A&AS, 138, 465
Gao, Y., & Dai, Z.-G. 2010, RAA, 10, 142
Ghirlanda, G., Ghisellini, G., Salvaterra, R., et al. 2013, MNRAS, 428, 1410
Graff, P. B., Lien, A. Y., Baker, J. G., & Sakamoto, T. 2015, arXiv:1509.01228
Graham, J. F., & Fruchter, A. S. 2013, ApJ, 774, 119
Graham, J. F., & Fruchter, A. S. 2015, arXiv:1511.01079
Graham, J. F., Fruchter, A. S., Kewley, L. J., et al. 2009, in AIP Conf. Proc. 1133, Gamma-Ray Burst: Sixth Huntsville Symposium, ed. C. Meegan, C. Kouveliotou, & N. Gehrels (Melville, NY: AIP), 269
Graham, J. F., Fruchter, A. S., Levesque, E. M., et al. 2015, arXiv:1511.00667
Greiner, J., Krühler, T., Klose, S., et al. 2011, A&A, 526, A30
Guetta, D., Piran, T., & Waxman, E. 2005, ApJ, 619, 412
Hanish, D. J., Meurer, G. R., Ferguson, H. C., et al. 2006, ApJ, 649, 150
Hopkins, A. M., & Beacom, J. F. 2006, ApJ, 651, 142
Horiuchi, S., Beacom, J. F., & Dwek, E. 2009, PhRvD, 79, 083013
Horiuchi, S., Beacom, J. F., Kochanek, C. S., et al. 2011, ApJ, 738, 154
Iwamoto, K., Mazzali, P. A., Nomoto, K., et al. 1998, Natur, 395, 672
Kaneko, Y., Bostancı, Z. F., Göğüş, E., & Lin, L. 2015, MNRAS, 452, 824
Kelly, P. L., & Kirshner, R. P. 2012, ApJ, 759, 107
Kobulnicky, H. A., & Kewley, L. J. 2004, ApJ, 617, 240
Levesque, E. M., Berger, E., Kewley, L. J., & Bagley, M. M. 2010a, AJ, 139, 694
Levesque, E. M., Kewley, L. J., Berger, E., & Jabran Zahid, H. 2010b, AJ, 140, 1557
Levesque, E. M., Kewley, L. J., Graham, J. F., & Fruchter, A. S. 2010c, ApJL, 712, L26
Li, W., Chornock, R., Leaman, J., et al. 2011, MNRAS, 412, 1473
Lien, A., & Fields, B. D. 2009, JCAP, 1, 47
Lien, A., Sakamoto, T., Gehrels, N., et al. 2014, ApJ, 783, 24
Lien, A., Sakamoto, T., Gehrels, N., et al. 2015, ApJ, 806, 276
Modjaz, M., Kewley, L., Kirshner, R. P., et al. 2008, AJ, 135, 1136
Ofek, E. O., Cenko, S. B., Gal-Yam, A., et al. 2007, ApJ, 662, 1129
Perley, D. A., Cenko, S. B., Bloom, J. S., et al. 2009, AJ, 138, 1690
Perley, D. A., Levan, A. J., Tanvir, N. R., et al. 2013, ApJ, 778, 128
Perley, D. A., Tanvir, N. R., Hjorth, J., et al. 2015, arXiv:1504.02479
Pian, E., Amati, L., Antonelli, L. A., et al. 1999, A&AS, 138, 463
Piran, T. 2005, NCimC, 28, 373
Racusin, J. L., Liang, E. W., Burrows, D. N., et al. 2009, ApJ, 698, 43
Robertson, B. E., & Ellis, R. S. 2012, ApJ, 744, 95
Ryan, G., van Eerten, H., MacFadyen, A., & Zhang, B.-B. 2015, ApJ, 799, 3
Salpeter, E. E. 1955, ApJ, 121, 161
Salvaterra, R., Campana, S., Vergani, S. D., et al. 2012, ApJ, 749, 68
Salvaterra, R., & Chincarini, G. 2007, ApJL, 656, L49
Stanek, K. Z., Dai, X., Prieto, J. L., et al. 2007, ApJL, 654, L21
Wanderman, D., & Piran, T. 2010, MNRAS, 406, 1944
Wolf, C., & Podsiadlowski, P. 2007, MNRAS, 375, 1049
Yates, R. M., Kauffmann, G., & Guo, Q. 2012, MNRAS, 422, 215
Yuan, T.-T., Kewley, L. J., & Richard, J. 2013, ApJ, 763, 9
Yüksel, H., Kistler, M. D., Beacom, J. F., & Hopkins, A. M. 2008, ApJL, 683, L5
Zahid, H. J., Geller, M. J., Kewley, L. J., et al. 2013, ApJL, 771, L19